

Phononic Self energy effects and superconductivity in CaC_6

A. Sanna^{1,2}, S. Pittalis³, J. K. Dewhurst^{1,2}, M. Monni⁴, S. Sharma^{1,2}, G. Ummarino⁵, S. Massidda⁴ and E. K. U. Gross^{1,2}

¹ *Max-Planck-Institut für Mikrostrukturphysik, Weinberg 2, D-06120 Halle (Germany)*

² *European Theoretical Spectroscopy Facility (ETSF)*

³ *University of Missouri, 1800 University Ave Columbia, MO (USA)*

⁴ *Dipartimento di Scienze Fisiche, Università degli Studi di Cagliari, Cagliari (Italy) and*

⁵ *C.N.I.S.M. Dipartimento di Fisica Politecnico di Torino, C.so Duca degli Abruzzi, 24, 10129 Torino (Italy)*

We study the graphite intercalated compound CaC_6 by means of Eliashberg theory, focusing on the anisotropy properties. An analysis of the electron-phonon coupling is performed, and we define a minimal 6-band anisotropy structure. Comparing with Superconducting Density Functional Theory (SCDFT) the condition under which Eliashberg theory is able to reproduce the SCDFT gap structure is determined, and we discuss the role of Coulomb interactions. The Engelsberg-Schrieffer polaron structure is computed by solving the Eliashberg equation on the Matsubara axis and analytically continuing it to the full complex plane. This reveals the polaronic quasiparticle bands anisotropic features as well as the interplay with superconductivity.

PACS numbers: 74.25.Jb, 74.25.Kc, 74.70.Ad

The electron-phonon interaction (EPI) leads to many significant physical phenomena in solids (notably, superconductivity), and has therefore been studied extensively both in model systems and in real materials. One interesting aspect of EPI is the formation of a coupled electron-phonon system with new interesting features, such as the appearance of polaronic sub-bands branching from the main electronic bands. Recent developments of angle-resolved photoemission spectroscopy (ARPES) allow for the investigation of the fine details of the electronic structure and, therefore, the effects of EPI on the low energy part of the spectral function. The theoretical background to deal with metallic polarons has been laid down by Engelsberg and Schrieffer (ES)¹, who used a field theoretical approach combined with either Einstein or Debye models to mimic the optical and acoustic parts of phonon spectra. Clearly, because of the computational complexity involved, a proper account of the material specific electronic and phononic structures could not be reached until very recently. Eiguren et al.² and Eiguren and Ambrosch-Draxl³ studied the effect of EPI on the electron self-energy in Be surface and in the 1×1 H/W(110) surface respectively, following the approach of ES.

In superconductors EPI eventually leads to the formation of a superconducting gap as soon as the system is cooled below the critical temperature T_c . The extension of the ES theory to the superconducting state is given by Eliashberg theory for strong coupled superconductors^{4,5}. The main properties of the spectral function in the superconducting state have been reported by Scalapino^{5,6}, and more recently have been studied in order to compare with ARPES data on high-temperature superconductors⁷⁻⁹. However no attempt has been reported so far, to the best of our knowledge, to focus on polaronic effects in the superconducting state of phononic superconductors from a purely first principles approach. The formation of a gap

in the electronic excitation energies, and the doubling of the spectra with the creation of Bogoliubov branches is expected to interplay with polaronic effects.

In order to investigate these effects, we will apply Eliashberg⁴ methods to the graphite intercalation compound CaC_6 . This system has attracted considerable interest in the last few years, mostly because of the attracting possibility of tuning the physical properties¹⁰. It is possible to change the intercalating atom or the geometry of the system to vary the conductivity from the semimetallic graphite¹¹, to a metal and in some interesting cases a superconductor¹²⁻¹⁵ as soon as the electron phonon coupling becomes strong enough¹⁶⁻¹⁹. In particular CaC_6 is the graphitic compound with the highest superconducting critical temperature observed so far (11.5 K). Superconductivity has been successfully explained by the electron phonon coupling provided both by C and Ca phonon modes^{16,20}. This coupling is strongly anisotropic, with C and Ca related phonons acting selectively and in a different way on the multiple Fermi surface (FS) sheets of the system²¹. These peculiarities of the EPI in CaC_6 make this system particularly interesting in view of possible reflections on the polaronic structure.

This work is devoted to the study of CaC_6 , both in the normal and in the superconducting states. The behaviour of ES polarons will be analyzed by a detailed study of the electronic self-energy, including electron-phonon contributions. In particular, the anisotropic structure originating from the anisotropic electron-phonon coupling of CaC_6 will be investigated. Most importantly, it will be shown how polaronic branches change in the superconducting state below the critical temperature T_c .

I. METHODS

In this work the theoretical framework of Eliashberg theory^{4,5,22,23} is used. A 2×2 Nambu Green's function is defined:

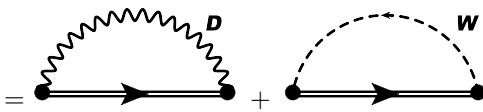
$$\bar{G}(\mathbf{k}, i\omega_n) = \begin{pmatrix} G(\mathbf{k}, i\omega_n) & -F(\mathbf{k}, i\omega_n) \\ -F^*(\mathbf{k}, i\omega_n) & G(\mathbf{k}, -i\omega_n) \end{pmatrix}, \quad (1)$$

where $G(\mathbf{k}, i\omega_n)$ and $F(\mathbf{k}, i\omega_n)$ are, respectively, the normal and Gor'kov Green's functions in reciprocal space and on the fermionic Matsubara's points $\omega_n = \pi(2n+1)k_B T$ (T being the temperature and k_B the Boltzmann constant). Following a well established procedure we choose as a reference non-interacting starting point the Kohn-Sham system, that provides the non interacting Green's function $\bar{G}_0(\mathbf{k}, i\omega_n) = [i\omega_n \sigma_0 - \xi_{\mathbf{k}} \sigma_3]^{-1}$. Where σ_j are the Pauli matrices and $\xi_{\mathbf{k}}$ the Kohn-Sham eigenvalues. The interacting Green's function is obtained via Feynman-Dyson perturbation theory:

$$[\bar{G}(\mathbf{k}, i\omega_n)]^{-1} = [\bar{G}_0(\mathbf{k}, i\omega_n)]^{-1} - \bar{\Sigma}(\mathbf{k}, i\omega_n), \quad (2)$$

The following approximation of the electronic self energy is used:

$$\begin{aligned} \bar{\Sigma}(\mathbf{k}, i\omega_n) = -k_B T \sum_{\mathbf{k}', n'} \sigma_3 \bar{G}(\mathbf{k}', i\omega_{n'}) \sigma_3 \times & \quad (3) \\ \left[\sum_{\nu} |g_{\mathbf{k}, \mathbf{k}', \nu}|^2 D_{\nu}(\mathbf{k} - \mathbf{k}', i\omega_n - i\omega_{n'}) + \sigma_1 W(\mathbf{k} - \mathbf{k}') \right] \end{aligned}$$



where W is an effective static electron-electron interaction (that does not account for a phonon mediated response, see below); D is the phonon propagator $-2\omega_{\mathbf{q}, \nu}/(\omega_n^2 + \omega_{\mathbf{q}, \nu}^2)$; $g_{\mathbf{k}, \mathbf{k}', \nu}$ are the electron phonon matrix elements²⁴ between states with wavevector \mathbf{k} and \mathbf{k}' and due to a phonon mode of index ν and wavevector $\mathbf{q} = \mathbf{k} - \mathbf{k}'$; while $\omega_{\mathbf{q}, \nu}$ is the frequency of the mode. The σ_1 factor in front of W accounts for the fact that exchange and correlation effects are already included in a reliable way with $\bar{G}_0(\mathbf{k}, i\omega_n)$ ²⁵, therefore only off-diagonal contributions from W are retained in $\bar{\Sigma}$.

The phononic structure also relies on the Kohn-Sham approach to density functional theory, and is obtained via linear response²⁴ in the Born Oppenheimer approximation. This method is known to give very good agreement with the measured phononic branches, at least for standard metals and insulators²⁴.

The treatment of the Coulomb term needs extra care. Within Eliashberg theory an arbitrary cut-off in \mathbf{k} space is needed in order to avoid serious convergency problems in the Matsubara summation^{5,26}. A conventional way to deal with this problem is to define an energy cutoff, and also to assume that the product of W and the density of

states is constant: $\mu = WN$ (N being the density of states per spin at the Fermi energy). This quantity can be calculated for example in the RPA approximation^{21,27,28}. The cut-off energy is chosen to be of the order of the Fermi energy. The Matsubara summation can then be performed, and the resulting critical temperatures are usually in reasonable agreement with experiments^{22,29}. The constraint of constant μ also allows for the cutting of the Matsubara integration at a low energy and then performing the high energy part of the integration in an analytic way^{5,26,30} with a rescaled interaction. A renormalized μ (denoted μ^*) is then used with a restricted energy window. For a purely repulsive interaction μ^* is always smaller than μ .

The self energy in Eq. (3) is \mathbf{k} -point dependent, and leads to computationally very expensive anisotropic Eliashberg's equations. An additional approximation can then be made by treating the system in a semi-isotropic approximation in which the Fermi surface is divided into portions (that we will refer to as Fermi surface sheets). In each part, the electron-phonon coupling is averaged as is the inter-part one. It is therefore possible to integrate out the explicit \mathbf{k} -dependence of the phononic part of $\bar{\Sigma}$ retaining only a *multiband* resolution. In this work the word multiband is used in the sense of multiple Fermi surface portions. In this way it is possible to simplify the equations, retaining a minimal anisotropic structure that accounts for the properties.

The self energy Σ on the J-Fermi surface sheet is expanded in the basis of Pauli matrices:

$$\Sigma_J(n) = i\omega_n [1 - Z_J(n)] \sigma_0 + \Delta_J(n) Z_J(n) \sigma_1 \quad (4)$$

neglecting those terms which result only in a shift of the Fermi level. This corresponds to the following Green's function solution of the Dyson equation:

$$\bar{G}_J(\mathbf{k}, i\omega_n) = \frac{-\begin{pmatrix} i\omega_n Z_J(n) + \xi_{J\mathbf{k}} & \Delta_J(n) Z_J(n) \\ \Delta_J(n) Z_J(n) & i\omega_n Z_J(n) - \xi_{J\mathbf{k}} \end{pmatrix}}{(Z_J(n)\omega_n)^2 + \xi_{J\mathbf{k}}^2 + \Delta_J^2(n) Z_J^2(n)}, \quad (5)$$

where $\xi_{J\mathbf{k}}$ are the Kohn-Sham eigenvalues (relative to the Fermi energy) corresponding to the electronic band that leads to the J-Fermi surface.

Using Eqs. (4) and (5) the Dyson equation (2) is then rewritten as a set of coupled self consistent equations named after Eliashberg^{4,5,22,29}:

$$Z_J(n) = 1 + \frac{\pi k_B T}{i\omega_n} \sum_{m, J'} \lambda_{JJ'}(n, m) \frac{i\omega_m Z_{J'}(m)}{R_{J'}(m)} \quad (6)$$

$$\Delta_J^{ph}(n) = \pi k_B T \sum_{m, J'} \lambda_{JJ'}(n, m) \frac{\Delta_{J'}(m) Z_{J'}(m)}{R_{J'}(m)} \quad (7)$$

$$\Delta_J^C(n) = -\pi k_B T \sum_{m, J'} \mu_{JJ'}^* \frac{\Delta_{J'}(m) Z_{J'}(m)}{R_{J'}(m)} \quad (8)$$

$$R_J(n) = \sqrt{(\omega_n^2 + \Delta_J^2(n)) Z_J^2(n)} \quad (9)$$

$$\lambda_{JJ'}(n, m) = \int d\omega \frac{2\omega \alpha^2 F_{JJ'}(\omega)}{(\omega_n - \omega_m)^2 + \omega^2} \quad (10)$$

where $\Delta_J = \Delta_J^{ph} + \Delta_J^C$ is the total superconducting gap accounting for phononic and Coulombic contributions on the J -th Fermi surface sheet and at frequency ω_n . $Z_J(n)$ is the phononic mass enhancement term that enters the diagonal part of the electronic self energy. It contributes both in the superconducting and in the normal state. We notice that the mass enhancement function is phononic as we assumed that all the diagonal contributions coming from electron-electron Coulomb interaction are properly accounted for in the Kohn-Sham system and are not double counted. One can see also that the μ^* is indicated as Fermi-surface dependent. Concerning the unrenormalised μ , it has been shown that, at the RPA level²⁸, the Coulomb potential W is also Fermi surface dependent. However, one has to bare in mind that the Coulomb renormalization mechanism smooths out this anisotropy through an integration over a large energy window. In practice, this can be seen by comparing with superconducting density functional theory results^{21,28}, that include Coulomb effects in a fully *ab-initio* anisotropic way, and has also been confirmed by experimental measurements^{31–36}. We will see that this comparison demonstrates that the multigap anisotropic structure obtained in SCDFT is well reproduced in Eliashberg theory only if a homogeneous (band independent) Coulomb coupling is used. This means that $\mu_{JJ'} = \mu N_J / N$ retains only a very basic structure given by the density of states $N_J = \sum_{\mathbf{k} \in J} \delta(\xi_{\mathbf{k}})$. In this work, the remaining parameter μ will not be calculated but adjusted to obtain the correct experimental critical temperature (T_c) of 11.5 K.

The sum over Matsubara's frequencies is cut off and ranges from $-\omega_c$ to ω_c where ω_c is chosen in such a way that the phononic part of the Eliashberg gap function Δ^{ph} is negligible outside this energy window while, as discussed above, in the purely electronic part, the presence of such a cut off is accounted by the use of μ^* . $\alpha^2 F_{JJ'}(\omega)$ appearing in Eq. (10) is the band-resolved Eliashberg function defined as:

$$\alpha^2 F_{JJ'}(\omega) = \frac{1}{N_J} \sum_{\substack{\mathbf{k} \in J \\ \mathbf{k}' \in J'}} \delta(\xi_{\mathbf{k}}) \delta(\xi_{\mathbf{k}'}) \delta(\omega - \omega_{\mathbf{q},\nu}) |g_{\mathbf{k},\mathbf{k}'}^{\nu}|^2 \quad (11)$$

This quantity is the result of averaging the electron-phonon interaction over Fermi surface areas discussed above.

Once the gap function $\Delta_J(n)$ and the mass renormalization function $Z_J(n)$ have been obtained on the imaginary axis solving the Eliashberg equations (6)–(10), they can be efficiently continued to the real axis via Padé's approximant technique^{37–39}. This allows the computation of the real-axis retarded Green's Function. In particular, we will deal with $G := \bar{G}^{11}$, given by:

$$G_J(\mathbf{k}, \omega) = \frac{\omega Z_J(\omega) + \xi_{J\mathbf{k}}}{[\omega Z_J(\omega)]^2 - \xi_{J\mathbf{k}}^2 - [\Delta_J(\omega) Z_J(\omega)]^2}, \quad (12)$$

with the corresponding spectral function defined as:

$$A_J(\mathbf{k}, \omega) = \frac{1}{\pi} \text{Im}G_J(\mathbf{k}, \omega). \quad (13)$$

It is also possible to define a quasi-particle spectrum, by searching for local minima of the function:

$$z - \frac{\sqrt{\xi_{J\mathbf{k}}^2 + [\Delta_J(z) Z_J(z)]^2}}{Z_J(z)} \quad (14)$$

in the complex plane. The real part of the pole coordinate z_p gives its position on the energy axis, while its lifetime is given by the inverse of its imaginary part.

II. COMPUTATIONAL DETAILS

Electronic eigenvalues, phonon frequencies and electron-phonon matrix elements were calculated using the ESPRESSO pseudopotential based package^{40,41}. All calculations were done using the GGA (generalized gradient approximation) with the Perdew-Wang⁴² parameterization for the exchange correlation functional. Ultrasoft pseudopotentials⁴³ were used. A 30 Ry cut-off has been fixed for the planewave expansion of the wavefunctions and 300 Ry for the electronic charge. The Brillouin zone was sampled with a $6 \times 6 \times 6$ k-point grid, and electron-phonon matrix elements obtained on a $10 \times 10 \times 10$ grid. More details can be found in reference 21.

The double Brillouin zone integration appearing in the definition of the band resolved Eliashberg functions in Eq. (10) has been evaluated with a Metropolis integration scheme. Random \mathbf{k} -points are generated on the Brillouin zone, then each \mathbf{k} -point is accepted or rejected with a probability depending on $\xi_{\mathbf{k}}$, and its weight set as inversely proportional to the acceptance probability. We used a set of about $2 \cdot 10^4$ accepted \mathbf{k} -points per band. Then electron-phonon matrix elements on this random mesh are obtained via interpolation from those calculated on the regular grid.

Eliashberg equations were solved using a 2500 meV cut-off of the Matsubara frequencies, with the cut-off ω_c for the Coulomb interaction chosen as 500 meV. Both parameters are much larger than the maximum phonon frequency of CaC₆ which is about 200 meV. The number of Matsubara points at each temperature is fixed by this cut-off, and the M Matsubara points on the positive imaginary axis are used to construct (M, M) Padé's approximants which were used for analytic continuation⁴⁴.

III. RESULTS AND DISCUSSION

A. Properties of the electron phonon coupling

We calculated the Eliashberg function defined by Eq. (11), in the isotropic approximation, using three FS

sheets and then six FS sheets (see figure and caption on Tab. I). In the first case, the electron-phonon coupling is assumed to be isotropic therefore it has been averaged over the full surface. In the second case, the three portions of Fermi surface have been separated in: 1) external π portion of the Fermi surface, shown in the central panel of Fig. 5, this Fermi Surface comes from the band indicated by a full blue line; 2) Ca sphere, that is the nearly spherical Fermi surface due to interlayer states; 3) π -prism, that is a two dimensional FS having the shape of a hexagonal prism which crosses the Ca-sphere. The six FS sheet division is somewhat arbitrary but is guided mostly by the structure of the electron-phonon coupling, in order to maximize coupling differences between the bands. The above named π external FS has been divided into a less coupled²¹ outer part with $|\mathbf{k}_{xy}| > 0.4$ a.u., and the rest. We will refer to these two portions respectively as 1a and 1b respectively. The Ca sphere has been cut into 2a with $|\mathbf{k}_z| < 0.18$ a.u., and the remaining part 2b. Similarly we define a 3a and 3b portions for the π -prism.

In Table I we collect the calculated density of states (DOS) at the Fermi level and intra as well as interband electron phonon couplings:

$$\lambda_{JJ'} = 2 \int d\omega \frac{\alpha^2 F_{JJ'}(\omega)}{\omega} d\omega \quad (15)$$

In the three band decomposition we see that CaC₆ is dominated by off diagonal coupling terms, especially the interband scattering term from states on the Ca sphere (2) to states on the π bands (1 and 3) because of a strong electron-phonon coupling in the former and large DOS in the latter. The full 3-band $\alpha^2 F_{JJ'}(\omega)$ matrix, as reported in Fig. 1, shows the distribution of the coupling among the phonon modes. We note that: band 2 is the one that couples strongly with Ca modes (giving a low frequency peak around 10 meV); band 1 couples mainly with high frequency stretching C modes (at 170 meV); band 3 instead is the one with the most homogeneous coupling, its intraband spectral function looks quite alike in shape to the total Eliashberg function. In principle we could define additional cuts of the FS reaching the full anisotropic \mathbf{k} -resolved limit of the Eliashberg functions, our 6 band division is already rich enough to describe all the main anisotropic features of the electron-phonon coupling.

B. Solution of Eliashberg's equations

The Eliashberg's equations are solved in three different ways: first by using an average coupling, in which the sums, appearing in Eq. 11, are performed over the full Brillouin Zone. We conventionally call this isotropic or one-band approximation. Second with a 3 bands coupling, as discussed in the previous section; and third with a 6 band coupling (also extensively discussed in the previous section), which we believe is able to describe in full the anisotropic properties of CaC₆.

	1	2	3						
1	0.301	0.136	0.257						
2	0.546	0.239	0.479						
3	0.427	0.198	0.367						
DOS	0.412	0.104	0.249						
	1a	1b	2a	2b	3a	3b			
1a	0.163	0.126	0.099	0.033	0.201	0.046			
1b	0.179	0.140	0.105	0.035	0.221	0.050			
2a	0.331	0.245	0.151	0.084	0.384	0.096			
2b	0.271	0.202	0.206	0.047	0.400	0.080			
3a	0.252	0.194	0.145	0.061	0.309	0.073			
3b	0.206	0.157	0.128	0.044	0.259	0.060			
DOS	0.250	0.176	0.075	0.031	0.200	0.056			

TABLE I: Three FS (top) and six FS (bottom) division, density of states and electron phonon coupling $\lambda_{JJ'}$. The first index runs over the columns. Isotropic DOS and λ are 0.787 and 0.870 respectively. DOS is given in states/eV/spin. The picture on the top represents the Fermi surface of CaC₆ the external green band is band 1; the internal blue sphere is 2, and the red hexagon that cuts the sphere is 3. The labels "a" and "b" correspond to the additional splitting used in the six portions division.

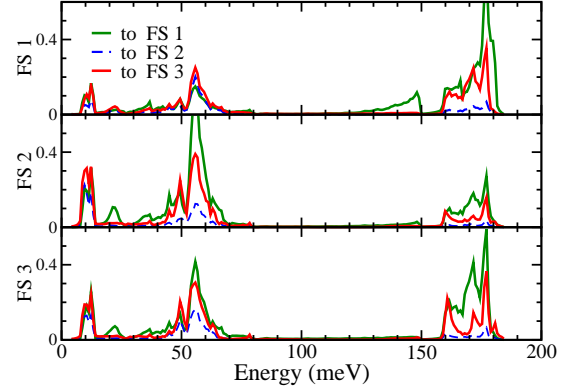


FIG. 1: (color online) Three band resolved $\alpha^2 F_{JJ'}(\omega)$ of CaC₆. The three panels refers to the starting FS from where the electron is scattered, while the three lines in each panel refer to the outgoing FS.

Unlike for MgB₂, T_c is not strongly affected by the multi-band character of CaC₆. In absence of Coulomb interaction the isotropic T_c is about 33.5 K, and just slightly higher in the 6-band case reaching 34 K. On the other hand, we observe a wide gap anisotropy. Fig. 2 contains the temperature dependence of the Eliashberg gap. The external Fermi surface (band 1) has a lower gap, slightly higher for its portion 1b, as expected. The top values of the gap are instead related to the 2a structure,

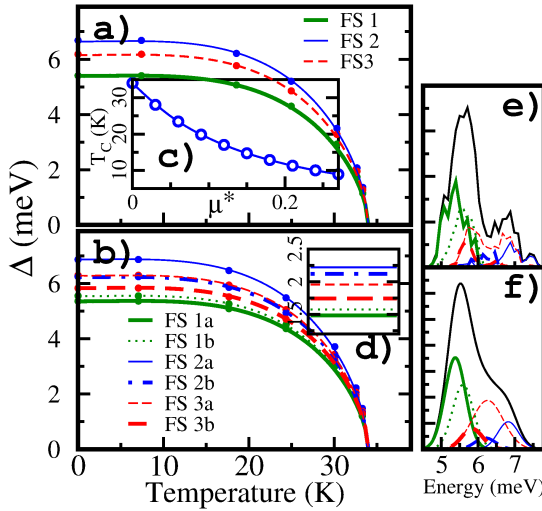


FIG. 2: (color online) Anisotropy of the superconducting gap, in a 3 FS division (a), and 6 FS division (b). In (a) the Dark green thick line is use for band 1; a blue thin line for 2; and the red dashed line for 3. In (b), dark green thick and dotted are used respectively for 1a and 1b; blue thin and thick dash dotted, for 2a and 2b; red thick dashed and thin dashed for 3a and 3b. (a) and (b) refer to phonon only calculations. Inset (c) shows the effect of including a Coulomb term, giving the Eliashberg T_c as a function of μ^* , see text for details. Inset (d) reports the low temperature multigap structure for $\mu^* = 0.21$. Panels (e) and (f) report the gap distribution functions (phonon only calculations) in the six FS division repsectively in SCDFT²¹ and Eliashberg (with a gaussian broadening applied).

the central part of the Ca FS Sphere. We comment here on the fact that, at the phononic level, the anisotropic structure obtained here compares extremely well with the one reported in Ref. (21) as obtained within SCDFT (see panels (e) and (f) in Fig. 2).

Upon including the Coulomb interaction, T_c decreases and reaches the experimental value of 11.5 K for $\mu^* \simeq 0.21$, in the 6-FS calculation (see inset c in Fig. 2). From now on we will refer to this case. As discussed in sec. I, SCDFT and this approach compare well only for a choice of the $\mu_{JJ'}$ matrix that corresponds to an isotropic effective coupling. Choosing $\mu_{JJ'}^*$ in this way, implies that the introduction of Coulombic effects reduces the critical temperature without strongly affecting the anisotropic structure of the superconducting gap. The only small difference we notice is that by including the Coulomb interaction the gap corresponding to the 2b portion of the FS becomes slightly larger than the 3a portion (see Fig. 2d). The choice of a homogeneous matrix is often done in Eliashberg theory, and this comparison somehow supports the validity of this approximation. However this can not be considered as a general rule, because we know, that in other cases, like in MgB₂^{45,46}, the structure of the Coulomb interaction is necessary to reproduce the correct gap anisotropy. Most likely because of the relatively weak interband interaction and the low Fermi energy of the σ bands in that case prevent an effi-

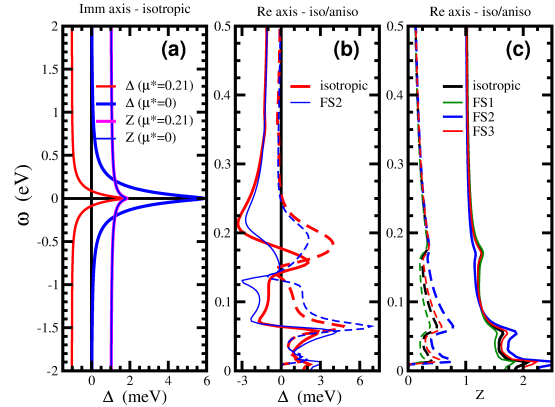


FIG. 3: (color online) Eliashberg functions. On the left (a) the superconducting gap and the mass renormalization function calculated solving the isotropic Eliashberg equations on the imaginary axis. In the center (b) the analytically continued gap function on the real axis. On the right (c) the analytically continued mass renormalization function. Full lines are used for real and dashed lines for imaginary parts.

cient Coulomb renormalization.

Both $\Delta(n)$ and $Z(n)$ are purely real on the Matsubara points. Their frequency dependence is shown in Fig. 3a, for the isotropic case. Few physical features can be distinguished in this form. Z has a value of $1+\lambda$ for small $|n|$ and then monotonically decreases to 1 at energies much larger than the available phonons. This behavior is almost independent of the values of μ^* and temperature. The Δ function also monotonically decreases from low to high energy. The low energy value is the fundamental superconducting gap, while in the high energy limits tends to Δ^C . Owing to the fact that we use an isotropic and static Coulomb potential, Δ^C is both independent of \mathbf{k} and from the Matsubara frequencies. More physical features emerge from the analytic continuation to real axis - in particular we see a three peak structure in both real and imaginary parts of Z that correlates with the peaks in the $\alpha_{JJ'}^2 F(\omega)$, and in turn will determine the quasiparticle spectrum.

C. Analysis of Self Energy Effects

1. Normal state, isotropic approximation

We discuss in this section the simplest case in which the Eliashberg equations are solved above the superconducting critical temperature. T_c being quite low with respect to the phonon energies, this case is almost identical to imposing the $\Delta = 0$ solution. In this section we use only the isotropic solutions of the Eliashberg's equations, and a parabolic band dispersion is assumed.

In the normal state, as discussed in Sec. I, no Coulomb effects will appear. The $Z(\omega)$ function obtained is shown in Fig. 3 c) (black line). Eq. (14) is solved in order

to obtain the quasiparticle dispersion curves reported in Fig. 4 (a). The main electronic band branches are in correspondance with the three main phononic peaks in the Eliashberg function, these electronic quasi-particles dressed by the EPI are polarons. However, these quasi-particles carry very little of the total spectral weight. In fact, most of the spectral weight is still localized near the bare electron dispersion line. This can be seen in Fig. 4 (b) where the spectral function is shown in the same energy/momentum window as the quasiparticle plot. In this case we only see how the main electron band acquires a finite lifetime, and instead of branching we see only kinks, corresponding to the three main peaks in the $\alpha^2 F(\omega)$. Here a very small fraction of spectral weight is transferred to the polaronic branches that are nearly dispersionless (slow). We observe only one dispersive branch, that goes to zero from about 50 meV. This structure also has a very short lifetime (~ 100 meV). All the other polaronic modes are strongly defined quasi-particles with a long lifetime (between 1 and 10 meV).

To move from a qualitative description to a more quantitative one, the spectral function $A(\omega)$ is examined (see Fig. 4) (c)). At $\mathbf{k} = \mathbf{k}_F$ more than 50% of spectral weight is accounted for by a single peak of infinite lifetime at E_F . This peak (single green line in Fig. 4 (c)) moves to higher energies with increasing \mathbf{k} -vector - slowly growing in width - up to an energy of about 10 meV where it merges with the polaronic branch due to low frequency Ca modes (long dashed blue line). Therefore, above this energy, the peak is broader (thick blue line), because the electrons can relax through emission of Ca phonons. This broad peak then behaves in a similar way as the narrow peak below 10 meV, i.e. it increases in energy with \mathbf{k} up until it merges with another polaronic band. This second one is due to low Frequency C modes (dot-dashed line), with an energy of about 50 meV. It becomes very broad (yellow short dashed curve), and is difficult to follow as it merges with the high frequency C mode. This behavior just described is very similar to the case of Einstein phonons (discussed by Engelsberg and Schrieffer¹), and is due to the three peaks structure of the $\text{CaC}_6 \alpha^2 F(\omega)$, or in other words, to the combined effect of two dimensionality of graphite along with the presence of weakly bound Ca ions. In CaC_6 at the isotropic level the self energy effects of the type given by Eq. (3) are therefore particularly simple.

2. Anisotropic features

The degree of complexity increases making use of the real band dispersions of CaC_6 ^{16,21}; at the same time also accounting for the presence of multiple Fermi surfaces, that couple with different phonon branches.

As shown by Fig. 5 c) d) e) f), the Ca band couples mostly with low frequency modes; has polaronic structures only up to 50 meV, and the only kink in the spectral function is at 50 meV. There is no kink at 10 meV

where the Ca modes are located because, before 10 meV, the spectral function is not visible, being just a sharp peak. The band that has most structures is the one that produces the prism-like FS (Fig. 5 g) h) i)) because it couples with all three sets of modes. While the external C FS couples mostly with hi-frequency C modes and shows only a weak kink around 160 meV. The polaronic branchings (Fig. 5 b', c', d', h' and i') have similar structures that were observed in the isotropic limit. Anisotropic features are less marked than observed in the spectral function because Eq. (14), used to highlight these features does not retain information about the spectral weight in the branches.

The spectral function in the superconducting phase is gapped. From the lower panels b*) c*) f*) g*) in Fig. 5, multigap features are clearly observed. Where the gap ranges from 1.5 meV around the point b in the band structure (Fig. 5 b*) to about 2.2 meV around c (Fig. 5 c*). At energies lower than 10 meV, where the Ca peak in the phonon spectrum is located and can play a role, the spectral function shows a textbook hyperbolic dispersion, signature of the Bogoliubov excitations²³, as compared with normal electronic excitations with linear band dispersion (see Fig. 5 c* and c#). Near the phonon energy of the Ca in-plane modes (from 10 to 15 meV), the Bogoliubov branches deviate from the linear asymptotic behaviour of the hyperbola. The trend along the main axis (the former electronic dispersion line) is similar to that observed in the normal state. Bogoliubov particles get dressed by EPI and acquire a large lifetime, and the polaronic branch acquires a small spectral weight compared to the main branch. The reflected line loses spectral weight as the distance from the Fermi surface increases, it is still clear how it deviates and forms a dispersionless Bogoliubov-Polaron that can be easily seen in the upper right and lower left corners of panel b* in Fig. 5.

IV. CONCLUSIONS

Superconductivity in the graphite intercalated compound CaC_6 using Eliashberg theory and SCDFT is studied. Within a multiband description and assuming a structureless Coulomb pseudopotential we performed a detailed analysis of the influence of strongly anisotropic electron-phonon coupling on the \mathbf{k} -dependence of the superconducting gap. Anisotropies computed with Eliashberg theory and SCDFT are in very good agreement with each other and with experiments³².

In this context, from the solution of the Eliashberg's equations we have shown how polaronic metallic bands emerge (within Engelsberg and Schrieffer theory¹) and have anisotropic features, over the different Fermi surface sheets.

We further report, for the first time, how Engelsberg-Schrieffer polarons evolve in going from the normal to the superconducting state. The interplay between su-

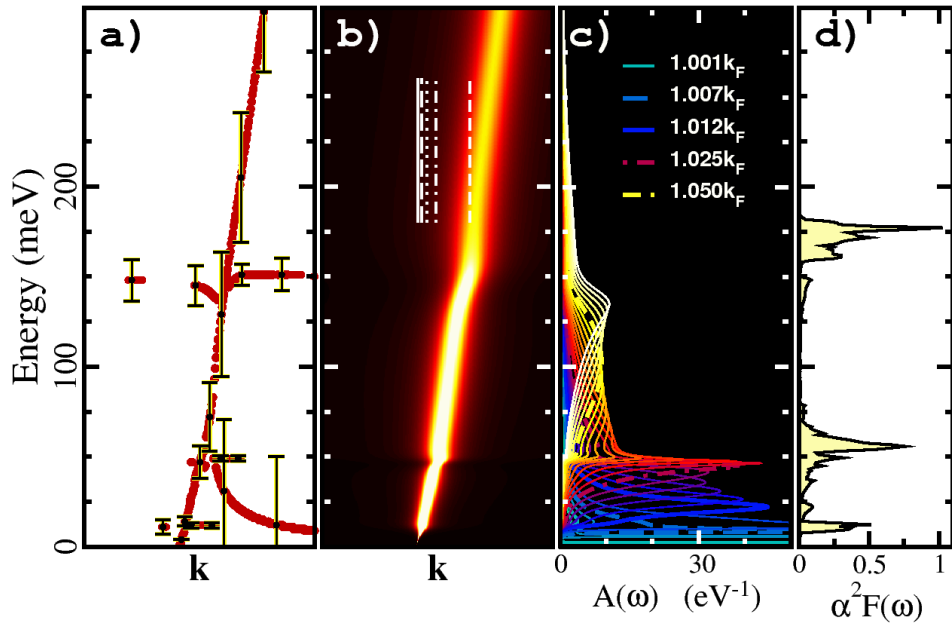


FIG. 4: (color online) Polaronic bands and spectral function for the normal state in the isotropic approximation. On panel a) the polaronic quasi-particle dispersion curves. This is the real part of z_p obtained from Eq. (14). The opposite of the imaginary part of the pole position z_p is reported for some points as error-bars (the full length of the error-bar is equal to $-\text{Im}(z_p)$, and gives the inverse lifetime of the state. On panel b) Spectral Function $A(k, \omega)$, the abscissa represent the $|\mathbf{k}|$ axis, and the point in which the Spectral Function crosses is \mathbf{k}_F . In ordinate the frequency axis. The color-scale goes from zero to about 15 eV^{-1} where we cut it off in order the structures of A to be enhanced. On panel c) the spectral function $A(k, \omega)$, for different values of the momentum. A few values are highlighted and correspond to \mathbf{k} values indicated in panel b). Panel d) shows the isotropic 1-band $\alpha^2 F(\omega)$ function to which the features of the quasiparticle spectrum and of the spectral function are related.

perconducting (Bogoliubov) excitations and polarons has also been studied. The small spectral weight of many structures provides a challenge for high resolution angle-resolved photoemission experiments.

V. ACKNOWLEDGMENTS

A. S. acknowledges useful discussions with A. Eiguren. S.P. acknowledges support through DOE grant DE-

FG02-05ER46203. S.M. acknowledges support by the Italian MIUR through Grant No. PRIN2008XWLWF9.

- ¹ S. Engelsberg and J.R. Schrieffer, Phys. Rev. **131**, 993 (1963).
- ² A. Eiguren, S. de Gironcoli, E.V. Chulkov, P.M. Echenique, and E. Tosatti, Phys. Rev. Lett. **91**, 166803 (2003).
- ³ A. Eiguren and C. Ambrosch-Draxl, Phys. Rev. Lett. **101**, 036402 (2008).
- ⁴ G. M. Eliashberg, Sov. Phys. JETP **11**, 696 (1960).
- ⁵ D. J. Scalapino, J. R. Schrieffer, and J. W. Wilkins, Phys. Rev. **148**, 263 (1966).
- ⁶ D. J. Scalapino, in *Superconductivity*, edited by R. D. Parks (Marcel Dekker, New York, 1969), Vol. 1, Chap. 10, p. 449.
- ⁷ A. W. Sandvik, D. J. Scalapino, and N. E. Bickers, Phys. Rev. B **69**, 094523 (2004).

- ⁸ T. P. Devereaux, A. Virosztek, and A. Zawadowski, Phys. Rev. B **59**, 14618 (1999).
- ⁹ X. J. Zhou, in *Handbook of High-Temperature Superconductivity*, edited by J. R. Schrieffer and J. S. Brooks (Springer, ADDRESS, 2007), Chap. 3.
- ¹⁰ M. S. Dresselhaus and G. Dresselhaus, Advances in Physics **51**, 1 (2002).
- ¹¹ D. Chung, Journal of Materials Science **37**, 1475 (2002), 10.1023/A:1014915307738.
- ¹² N. B. Hannay, T. H. Geballe, B. T. Matthias, K. Andres, P. Schmidt, and D. MacNair, Phys. Rev. Lett. **14**, 225 (1965).
- ¹³ T. E. Weller, M. Ellerby, S. S. Saxena, R. P. Smith, and T. N. Skipper, Nature Physics .

¹⁴ N. Emery, C. Hérold, M. d'Astuto, V. Garcia, Ch. Bellin, J. F. Marêché, P. Lagrange, and G. Loupias, Phys. Rev. Lett. **95**, 087003 (2005).

¹⁵ Gabor Csanyi, P. B. Littlewood, Andriy H. Nevidomskyy, Chris J. Pickard, and B. D. Simons, Nature Physics .

¹⁶ Matteo Calandra and Francesco Mauri, Phys. Rev. Lett. **95**, 237002 (2005).

¹⁷ I. I. Mazin, Phys. Rev. Lett. **95**, 227001 (2005).

¹⁸ Lilia Boeri, Giovanni B. Bachelet, Matteo Giantomassi, and Ole K. Andersen, Phys. Rev. B **76**, 064510 (2007).

¹⁹ J. S. Kim, L. Boeri, J. R. O'Brien, F. S. Razavi, and R. K. Kremer, Phys. Rev. Lett. **99**, 027001 (2007).

²⁰ Matteo Calandra and Francesco Mauri, Phys. Rev. B **74**, 094507 (2006).

²¹ A. Sanna, G. Profeta, A. Floris, A. Marini, E. K. U. Gross, , and S. Massidda, Phys. Rev. B **75**, 020511(R) (2007).

²² P. B. Allen and B. Mitrovic, *Solid State Physics*, edited by F. Seitz (Academic Press, Inc., New York, 1982), Vol. 37, p. 1.

²³ J. R. Schrieffer, *Theory of Superconductivity*, Vol. 20 of *Frontiers in Physics* (Addison-Wesley, Reading, 1964).

²⁴ S. Baroni, S. de Gironcoli, and A. Dal Corso, Rev. Mod. Phys. **73**, 562 (2001).

²⁵ Andrea Marini, Giovanni Onida, and Rodolfo Del Sole, Phys. Rev. Lett. **88**, 016403 (2001).

²⁶ P. Morel and P. W. Anderson, Phys. Rev. **125**, 1263 (1962).

²⁷ Chang-Youn Moon, Yong-Hyun Kim, and K. J. Chang, Phys. Rev. B **70**, 104522 (2004).

²⁸ S. Massidda S, F. Bernardini, C. Bersier, A. Continenza, P. Cudazzo, A. Floris, H. Glave, M. Monni, S. Pittalis, G. Profeta, A. Sanna, S. Sharma, and E.K.U. Gross, Supercond. Sci. Technol. **22**, 034006 (2009).

²⁹ J. P. Carbotte, Rev. Mod. Phys. **62**, 1027 (1990).

³⁰ C. R. Leavens and Fenton E. W., Solid State Comm. **33**, 597 (1979).

³¹ D Daghero and R S Gonnelli, Superconductor Science and Technology **23**, 043001 (2010).

³² R. S. Gonnelli, D. Daghero, D. Delaude, M. Tortello, G.A. Ummarino, V.A. Stepanov, J. S. Kim, R. K. Kremer, A. Sanna, G. Profeta, and S. Massidda, Phys. Rev. Lett. **100**, 207004 (2008).

³³ U. Nagel, D. Hühn, E. Joon, J. S. Kim, R. K. Kremer, and T. Röhm, Phys. Rev. B **78**, 041404 (2008).

³⁴ T. Shiroka, G. Lamura, R. De Renzi, M. Belli, N. Emery, H. Rida, S. Cahen, J.-F. Marêché, P. Lagrange and C. Hérold, New J. Phys., **13**, 013038 (2011).

³⁵ D. Daghero and R.S. Gonnelli, Supercond. Sci. Technol. **23**, 043001 (2010).

³⁶ C. Kurter, L. Ozyuzer, D. Mazur, J.F. Zasadzinski, D. Rosenmann, H. Claus, D.G. Hinks and K.E. Gray, Phys. Rev. B **76**, 220502(R) (2007).

³⁷ H.J. Vidberg and J.W. Serene, J. Low. Temp. Phys. **29**, 179 (1977).

³⁸ G.A. Baker Jr., *Essentials of Padé approximants* (Academic Press, 1975).

³⁹ C. M. Bender and S. A. Orszag, *Advanced Mathematical Methods for Scientists and Engineers* (Springer, 1999).

⁴⁰ ESPRESSO package: <http://www.pwscf.org/>.

⁴¹ Paolo Giannozzi et Al., Journal of Physics: Condensed Matter **21**, 395502 (2009).

⁴² J.P. Perdew and Y. Wang, Phys. Rev. B **45**, 13244 (1992).

⁴³ D. Vanderbilt, Phys. Rev. B **41**, 7892 (1990).

⁴⁴ Padé approximants were used to continue solutions of the Eliashberg's equations to the real axis. Very good agreement is observed in the full energy spectrum for the Z function. The analytically continued gap function $\Delta(\omega)$ shows some deviations from the exact solutions in the $\sim 0.1\text{eV}$ energy region. However Δ is important only for the meV scale, where the error is negligible.

⁴⁵ A. Floris, G. Profeta, N. N. Lathiotakis M. Lüders, M. A. L. Marques, C. Franchini, E. K. U. Gross, A. Continenza, and S. Massidda, Phys. Rev. Lett. **94**, 037004 (2005).

⁴⁶ A. Floris, A. Sanna, M. Lüders, G. Profeta, N. N. Lathiotakis, M. A. L. Marques, E.K.U. Gross, A. Continenza, and S. Massidda, Physica C **456**, 45 (2007).

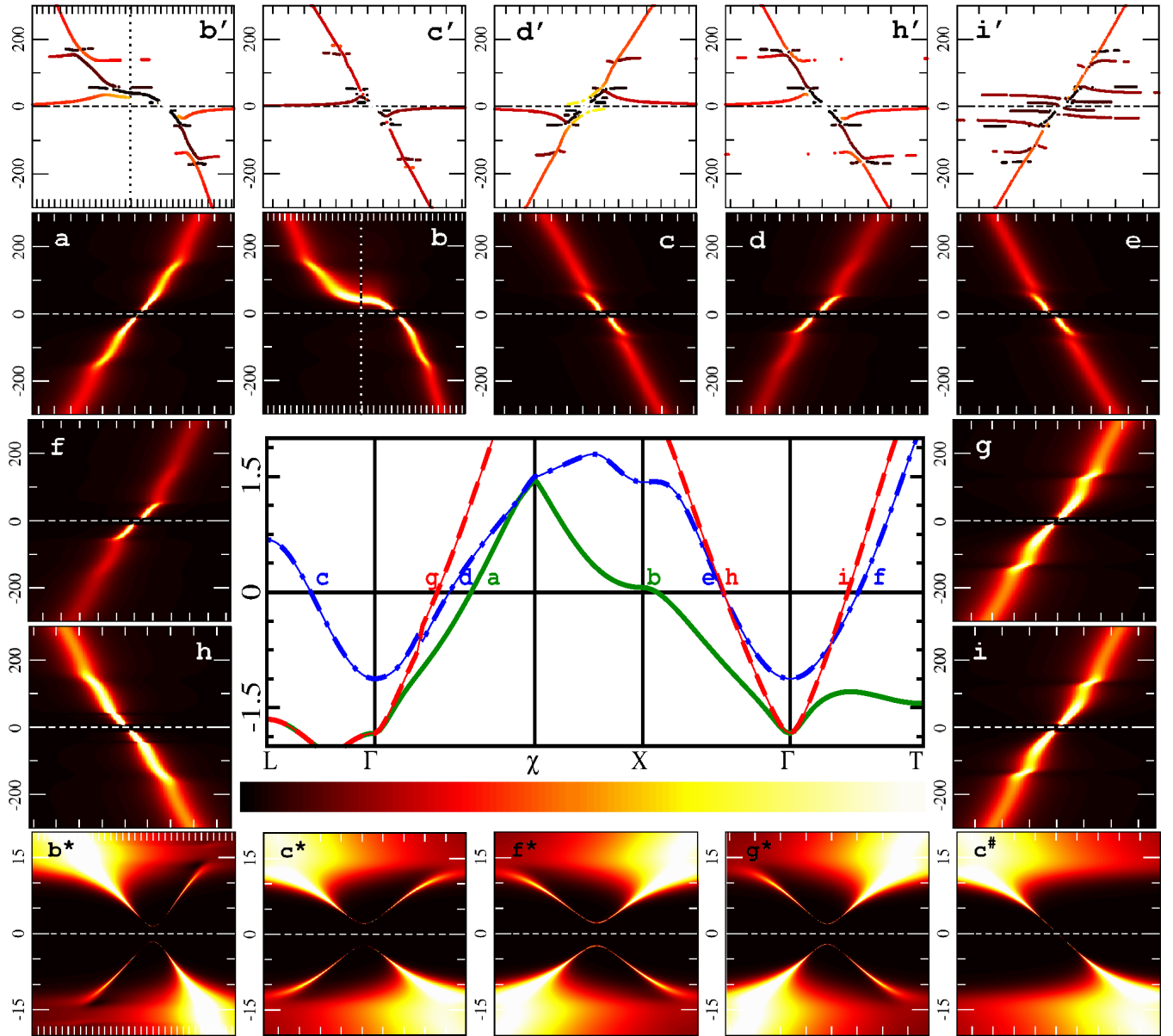


FIG. 5: (color online) Polaronic bands and spectral function for the anisotropic and superconducting state. Central panel, band structure of CaC_6 : the continuous green line is the external $\text{C}\pi$, the dot dashed blue line is the Ca interlayer band and the dashed red line is the internal cylindrical $\text{C}\pi$ band. Panels from **a** to **i**, spectral function near the Fermi Energy in a wide energy window of 300 meV. The letters correspond to the labeling of the crossing points in the central panel. The colorscale goes from zero (black) to 15 eV^{-1} (white), higher peaks in the spectral function have been cut off. Panels with a primed index show the quasiparticle spectrum (see text for details) that also show the polaronic branches together with the main electronic band. Colors are proportional to the linewidth of the quasiparticle state. Black corresponding to zero and yellow/white to about 0.1 eV. Panels **b***, **c***, **f*** and **h***, show a zoom of the spectral function near the Fermi energy in a narrow energy window of 20 meV, focusing on the superconducting gap (a logarithmic colorscale is used). Panel **c[#]**, same as **c***, but evaluated in the non-superconducting state.